A Detached-Eddy-Simulation study: Proper-Orthogonal-Decomposition of the wake flow behind a model wind turbine

IOP Conf. Series: Journal of Physics: Conf. Series **1104** (2018) 012005 doi:10.1088/1742-6596/1104/1/012005

A Detached–Eddy–Simulation study: Proper–Orthogonal-Decomposition of the wake flow behind a model wind turbine

J. Göing[1], J. Bartl[2], F. Mühle[3], L. Sætran[2], P.U. Thamsen[1]

Technical University of Berlin[1] (TUB), Norwegian University of Science and Technology[2] (NTNU), Norwegian University of Life Sciences[3] (NMBU)

Jan.Goeing@gmail.com

Abstract. In times of intense renewable energy development, the planning of wind farms and the improvement of their total efficiency has become a major field of research. A precise analysis of the velocity deficit, fluctuation load and the wake properties behind a turbine is essential to identify the optimal positioning and control of a wind farm cluster. Due to the increasing computer performance, numerical models have become an important tool for the precise analysis of the turbulent wake flow and for the optimization of the positioning of the turbine in a wind farm. In this study the wake characteristics are calculated with a Delayed-Detached-Eddy-Simulation (DDES) using a sliding mesh technique. The simulation is based on a 3D model wind turbine with a diameter of 0.89 m and a test area which corresponds to the wind tunnel geometry at the Department of Energy and Process Engineering at NTNU. A validation of DDES with an experimental Laser-Doppler–Anemometry (LDA) matches well with the results of the simulation. Furthermore, the coherent motions of vortex shedding in the near wake are detected with the Proper–Orthogonal-Decomposition (POD) technique while the significant frequencies are detected with a Power–Spectral–Density (PSD). These quantities describe the transition from coherent to turbulent motions in the wake and explain the influence of the downstream flow in detail. The investigation shows that the DDES computations are able to accurately predict the mean and turbulent wake flow behind a model wind turbine.

1. Introduction

In a wind farm cluster the downstream turbines exposed to reduced wind velocities, due to the upstream turbine's extraction of the kinetic energy from the wind. As a consequence, the area of the stream tube behind the turbine increases and a velocity deficit emerges. Furthermore, the turbines generate a highly turbulent wake flow causing fluctuating loads on downstream turbine.

Several analytical models are used to approximate the wake flow for the positioning of the turbines. However, the models have restricted boundary conditions, which influence the correctness of the estimation. Based on the increasing computer capacity, the Computational-Fluid-Dynamics (CFD) is an increasingly applied method for wake flow analysis. With CFD the wake flow can be calculated and the potential of the improvement of the wind farm can be determined.

In this study a high-fidelity CFD simulation of a model wind turbine in a wind tunnel is computed to investigate the downstream wake and to validate the results. The wake is calculated using the Large-Eddy-Simulation (LES) to produce accurate results. However, a study by Piomelli et al. [1] has shown the accurate resolution of an airfoil boundary layer requires a fine mesh for a LES. To

minimize and optimize the computer capacity a Delayed-Detached-Eddy-Simulation (DDES) technique by Spalart et al. [2] is used. In this method, the boundary layer is modelled with a Reynolds-Averaged-Navier-Stokes-Simulation (RANS) and the flow outside the boundary layers is simulated with a LES.

To compare the results with a measurement, the boundary conditions, the turbine and the test area are based on previous work by Bartl and Sætran [3]. The simulation includes the geometry of a three-bladed rotor with a hub, nacelle and tower. The rotating blades are generated by a sliding mesh technique. To analyse and discuss the results and the accuracy of the simulation, the velocity components and the turbulent kinetic energy (TKE) are compared to experimental data obtained by Laser-Doppler-Anemometry (LDA) [Bartl et al. [4]]. To get a detailed analysis and to investigate the limits of the simulation the modes inside of the wake are determined using Proper-Orthogonal-Decomposition (POD) to detect the coherent motions. In addition, the most significant frequencies are analysed in the wake flow by using a Power-Spectral-Density (PDS) analysis.

2. Methods

2.1. General information

In this investigation, the simulations are calculated with Ansys Fluent v17.2 on the high-performance computer VILJE at the NTNU. The segregated Pressure - Implicit with Splitting of Operators (PISO) solver is selected to calculate the equations. Based on the flow process a bounded central difference scheme is chosen for the discretization.

To compare the results, the same rotor is used as in previous studies by Bartl and Sætran [3]. The diameter D of the rotor is 0.89 m and the blades are designed based on the NREL S826 airfoil profile. The turbine is designed for a tip speed ratio of $\lambda = 6$ which results in a Reynolds number of Re = 100000 at the blade tips.

The computational domain has the same geometry as the wind tunnel of the Department of Energy and Process Engineering at the NTNU and is 2.7 x 1.8 x 11.0 m^3. The distance between the rotor and the inlet is 2D = 1.8 m. The time samples in the computations are recorded with a frequency of 2 kHz, corresponding to rotation by 3.81° in each time step. Furthermore, the simulation is calculated for a real time of 2 s and the evaluation is started after 0.7 s. An independency of the time step has been conducted.

2.2. Inflow conditions

In this report the simulation has a non-uniform shear flow as inflow condition. The turbulence intensity TI = 12% and the length scales $L_{uu} = 0.1$ m are generated with the spectral synthesizer. The algorithm should generate a TI of 10% in the ambient flow at the location of the rotor, due to the TI in the experiment by Bartl et al. [4].

2.3. Mesh configuration

The mesh consists of $55 \cdot 10^6$ elements and $30 \cdot 10^6$ nodes. It is divided in four different parts: rotor-, turbine-, wake- and tunnel-domain (see Figure 1). The rotor-domain rotates with the rotor and is coupled to the turbine-domain via the sliding mesh method.

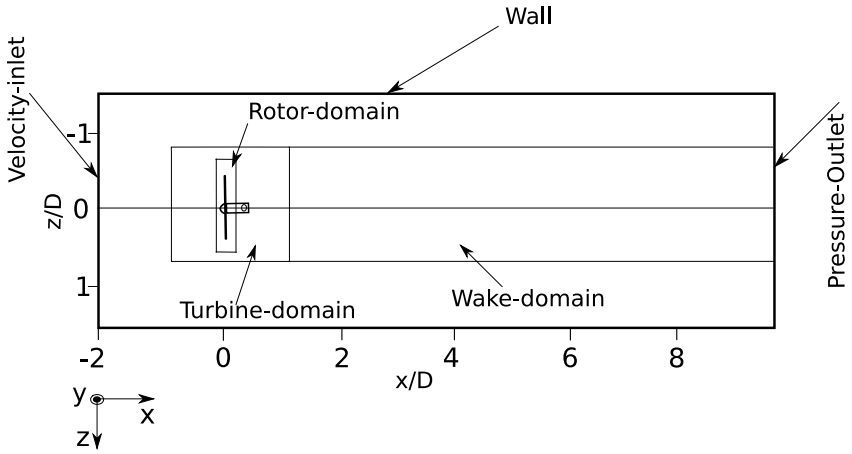

Figure 1. Geometry and mesh description of the test area and turbine

The thickness of a boundary layer on the blades is approximated through the boundary layer on a flat plate. To increase the computer performance and to optimize the number of the cells, the wall function is used for the velocity gradient inside of the boundary layer at the tip position. To implement the wall function in the boundary layer the unitless distance y_+ should be higher than 30. The distance to the first grid in the boundary layer is selected to $5 \cdot 10^{-4}$ m to achieve the value.

The refined wake-domain is approximated with the increasing stream tube. The grid should be able to resolve the Taylor micro scales λ_T and macro scales Λ. They can be computed with the autocorrelation method. In figure 2 the scales of the wake in streamwise direction are demonstrated in different positions. The length scales of the eddies increased after each location. The maximum of each curve is detected in a position z/D = ± 0.5 ± 0.1. The size of the eddies is between 6 and 12 mm. The macro scales are illustrated in the left diagram and have a size between 50 and 120 mm.

A grid independency study has been conducted.

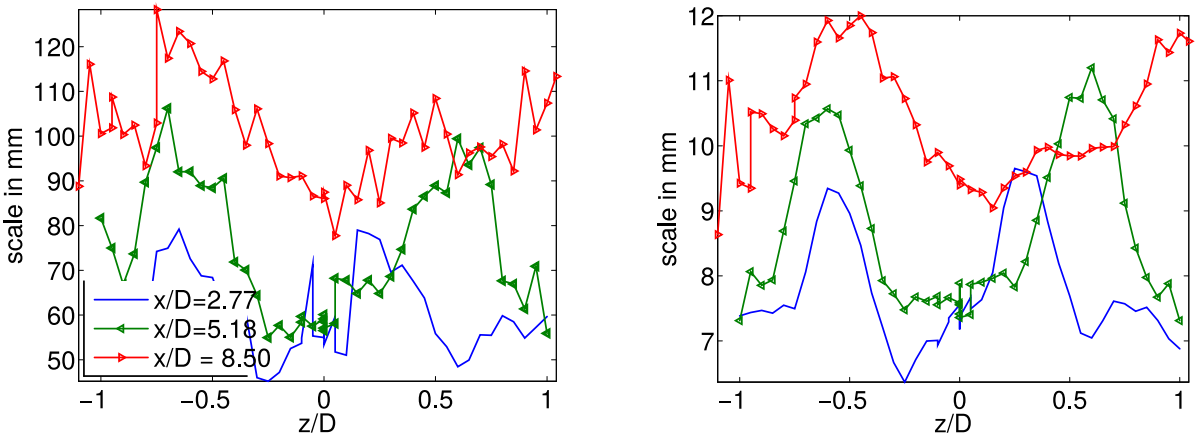

Figure 2. Length scales behind the turbine; (a): Taylor macro scales; (b) Taylor micro scales

2.4. Validation process

To evaluate the simulation, the mean velocity in x-direction (streamwise velocity u(x,t)), in y-direction (vertical velocity v(x,t)) and the TKE are compared to the LDA measurements in the location x/D=3 and 6. Based on the two components LDA measuring system (Bartl et al. [4]), the TKE is defined by following equation

$$k = \frac{1}{2} \cdot \left(\overline{u'^2} + 2 \cdot \overline{v'^2}\right).$$

The coherent motions and the significant frequencies are filtered out with a POD method by Chatterjee [5] and a PSD for a profound look at the accuracy of the results. The POD technique disassembles a snapshot matrix M of the flow field in x/D=1, 3 and 6. The streamwise velocity fluctuation u'(x,t) in each time step is included in the matrix M. The decomposition is based on the Singular-Value-Decomposition (SVD) according to the following equation

$$M = U \cdot \Sigma \cdot V^{T}.$$

Herein, the physical interpretation of the unitless matrix U, which includes the left eigenvectors, is the spatial mode. The diagonal matrices $\sum$ include the value of the eigenvalues σ, which describes the TKE. The matrix V, which includes the right eigenvectors with the unit m/s, is the time mode for the flow field. By phase averaging the angle between the highest time modes the coherent velocity $\tilde{u}(x,t)$ can be calculated, which is a part of the triple decompositions

$$u(x,t) = \bar{u}(x) + u'(x,t) + \tilde{u}(x,t).$$

To determine the dissipation process of the fluctuation load of 1p, a PSD is calculated on the first time modes.

3. Results

3.1. Flow field comparison

A general overview of the main results is visualized in figures 3 and 4. In both figures the normalized mean streamwise velocity u*, vertical velocity v* and TKE k* are compared to the LDA-measurement. The top row of the figures illustrates the results of the simulation and the row below shows the results of the corresponding LDA experiment by Bartl et al. [4].

The results in figure 3 are recorded at the downstream position x/D=3 and the general characteristics of the near wake behaviour are described. The rotor diameter of the turbine is represented as the black circle.

In the first column the normalized mean velocity u* is shown. The velocity reduction can be described as the velocity deficit behind the turbine. A circular structure with high velocity gradients in the centre and at the edge of the circle are shown. Also a nearly axissymmetrical velocity peak is detected inside of the deficit. The lowest velocity u* is under 0.5 and the fastest u* is about 0.8. Furthermore, the wake expands until r/D=0.6.

Compared to the simulation, a velocity deficit with lower velocity gradients at the edge and larger gradients in the centre is demonstrated in the flow field behind the turbine in the measurement row. Herein, the lowest normalized velocity inside of the deficit is about 0.5 and the fastest is in the range of 0.7. The area of the velocity deficit is nearly the same as in the simulation, with a higher impact on the negative y-direction until -0.6. In both results, the shear flow of the ambiance is pictured outside of the velocity deficit, which has an ordered velocity gradient in the simulation compared to the LDA-results.

In the second column the normalized mean vertical velocity v* is illustrated. In the diagram of the simulation three different velocity ranges are detected. Inside of the velocity deficit and in the negative z-direction the average velocity v* has a positive value (red/yellow) with a maximum about 0.2 and in the positive z-direction the average velocity v* has a negative value (blue) with a minimum about -0.2. These areas are connected with a steep velocity gradient and they represent a rotating process. The remaining part outside of the deficit has an average velocity v* about 0.0 (green). The second row shows the normalized mean vertical velocity v* of the measurement. In contrast to the simulation, the

velocity describes a rotation in the full y-z-plane of the wind tunnel. The maximum is about 0.1 and the minimum about -0.1 of the velocity v*.

Finally, the normalized TKE k* is presented in the third column. High levels of TKE indicate a high level of local shear in the flow. The TKE at the edge of the velocity deficit, with a value between 0.015 and 0.3 is illustrated in the first row of the simulation. The second row has a nearly constant level about 0.025. Finally, a significant difference of the shear is detected in ambient flow and inside of the deficit, which is higher than 0.01 in the measurement and lower than 0.01 in the simulation.

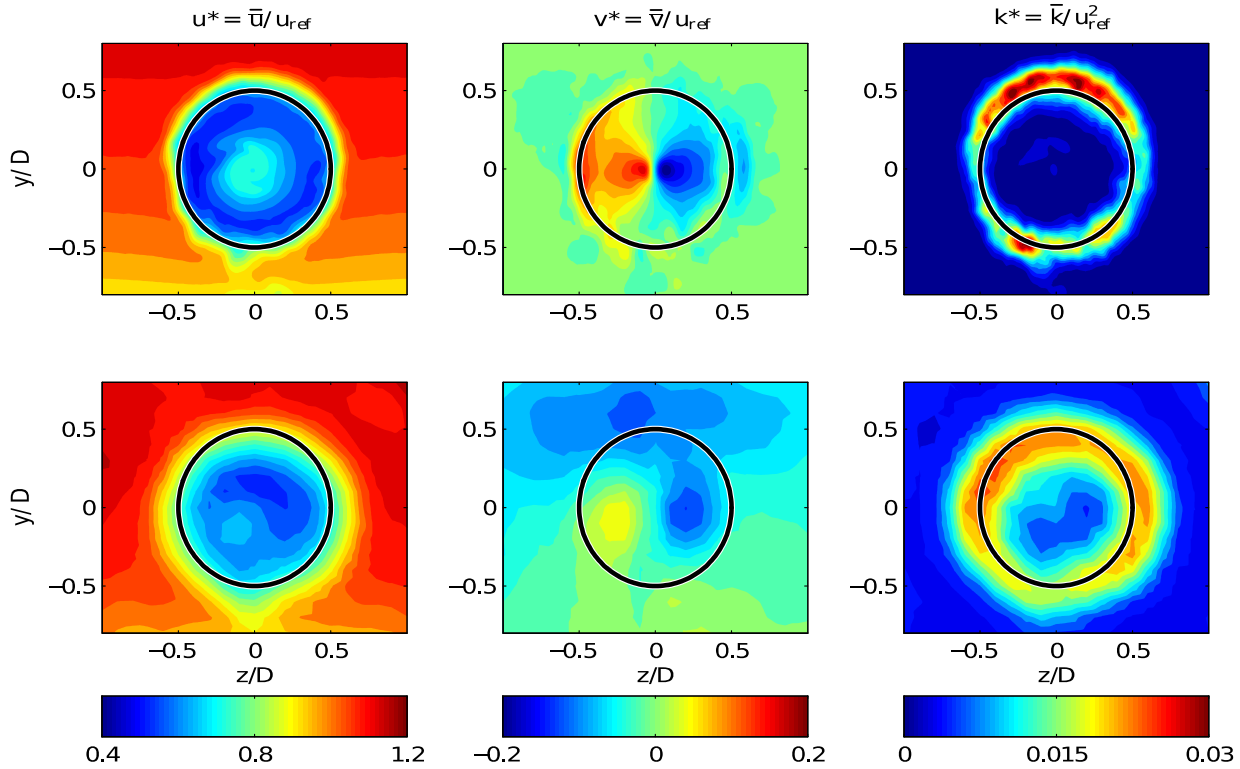

Figure 3. Different characteristics of the wake in y-z-plane at the location x/D=3. The black circle pictures the rotor diameter. Top: Simulation; Bottom: LDA; Left normalized mean streamwise velocity; Middle: normalized vertical velocity; Right: normalized TKE.

The general characteristics of the wake flow are pictured in figure 4 at the location x/D=6. In the first row the results of the simulation are illustrated and in the second row the results of the measurement are presented. A velocity deficit behind a turbine in the area until r/D=0.68 is shown in the results of the simulation in the first column. The velocity peak inside of the deficit has disappeared and the velocity gradients at the edge are larger compared to the location x/D=3. The minimum of the velocity level is about 0.6. The velocity u* of the measurement is illustrated in the second row. The impact of the deficit is detected between y/D=±0.6 and z/D=±0.7. The lowest velocity is at the same level as the simulation, though with a smaller area. This area is located in the center. Similar to the first row, the velocity peak disappeared. In contrast to the position x/D=3, the shape of the deficit has a higher fluctuation and u* has a less clear circular shape in both cases.

The vertical velocity v* is demonstrated in the second column. Similar to the previous downstream distance, a rotating flow field is presented in this column. The flow is only rotating inside of the velocity deficit area in the simulation. The maximum of the velocity is detected in the negative y-direction and is close to 0.1. The minimum is close to -0.1 and located in the positive direction. The average velocity in the ambient flow is similar to the location x/D=3 with a value of 0.0. The velocity

v* of the measurement is shown in the second row. Similar to the first position the ambient air of the y-z-plane is moved around. Apart from that, the maximum and minimum is about ±0.05.

The last column displays the TKE, which describes the turbulence of the flow field. Compared to the first position, the k* peaks merge together until the center of the simulation. The maximum is about 0.025 and has similar a structure as the measurement. The k* of the measurement has a maximum about 0.02 and a higher TKE in the ambient flow as the simulation. In both cases the average of the k* increased and the maximum decreased compared to the position x/D=3.

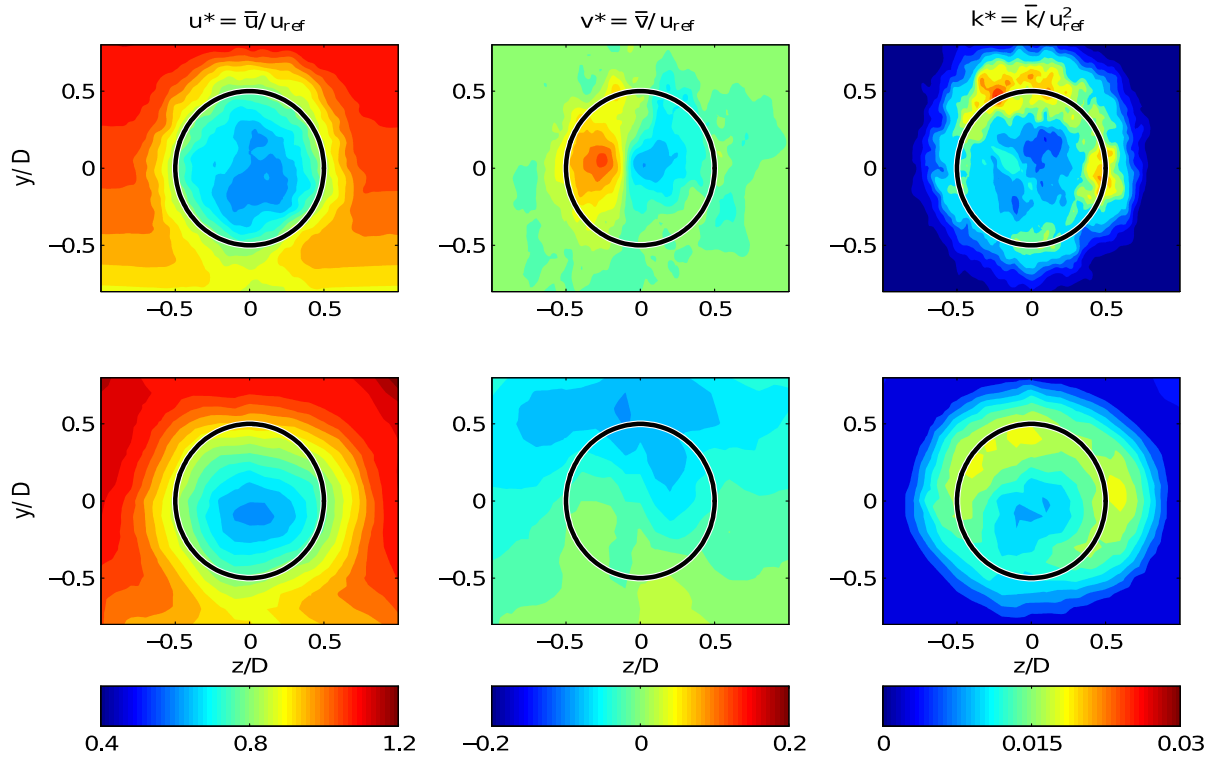

Figure 4. Different characteristics of the wake in y-z-plane at the location x/D=6. The black circle pictures the rotor diameter. Top: Simulation; Bottom: LDA; Left: normalized mean streamwise velocity; Middle: normalized vertical velocity; Right: normalized TKE.

3.2. Coherent motions and dissipation process of the fluctuation load

To investigate the coherent velocity $\tilde{u}(x,t)$ of the triple decomposition and the dissipation process of fluctuation load with the highest downstream range in the streamwise velocity u(x,t), the POD method is applied at the position x/D=1, 3 and 6.

After the decomposition of the snapshot matrix M, the eigenvalues of the flow field are included in the diagonal matrix Σ. The physical interpretation of the eigenvalues is the TKE, which are illustrated in the left diagram of figure 5 at the location x/D=1. The diagram displays the first 150 important normalized eigenvalues. A steep gradient at the beginning is visible in the curve. The normalized TKE of the first mode is 8% and of the second mode is 7%. Furthermore, the diagram explains that the first few modes have the highest impact on the total TKE and on the flow field. The right eigenvector (time mode V) includes information about the frequency spectrum. In the right diagram of figure 5 the normalized second time mode V_2^* over V_1^* is presented at the location x/D=1. A phase shifted behaviour between these both modes is described in the diagram by the dotted closed circle.

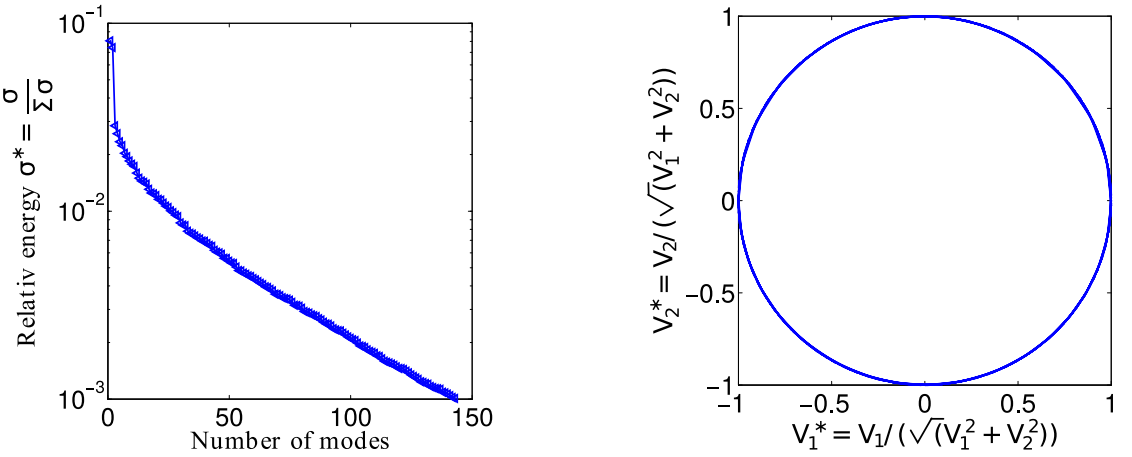

(a) (b)

Figure 5. POD analysis in x/D=1; (a) Relative energy of the modes; (b) Interaction between the first and second time modes.

Moreover, the circle in figure 5 can be used to calculate the phase angle between the first and second mode. The average of these angles is the phase average, which is necessary for the calculation of the coherent velocity $\tilde{u}(x,t)$.

The normalized coherent velocity $\tilde{u}^*$ of the streamwise velocity u(x,t) in the positions x/D=1, 3 and 6 are demonstrated in figure 6. The left diagram shows the velocity in x/D=1. Two circles next to the edge of the blades are detected. They are located between r/D=0.53 and r/D=0.63. The first circle (red/yellow) has a positive and the second (blue) a negative velocity. Furthermore, a significantly weaker $\tilde{u}(x,t)$ is detected in the centre of the wake. The two circles with changing signs are also shown in the diagram in the middle (x/D=3). They are located between r/D=0.42 and r/D=0.68. The lines of the circle are wider and have a higher spatial variation. The right diagram shows the coherent velocity in the position x/D=6. In contrast to the other locations, the clear circles are dispersed. However, the diagram shows also a changing sign in $\tilde{u}(x,t)$.

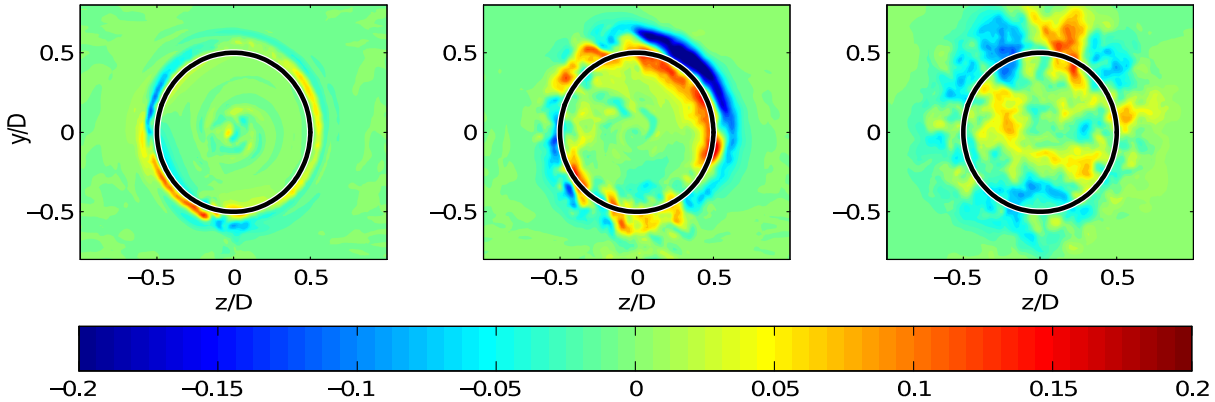

Figure 6. Coherent normalized streamwise velocity $\tilde{u}^*(x,t) = \tilde{u}/u_{ref}$ of the phase average between V_1 and V_2. The black circle pictures the rotor diameter. Left: x/D=1; Middle: x/D=3; Right: x/D=6.

Finally, the time modes include the fluctuation information of the streamwise velocity u(x,t) and can be used for a frequency analysis. The PSD over the logarithmic Strouhal ST number of the first

time mode V_1 in the locations x/D=1, 3 and 6 are shown in figure 7. The Strouhal number is the normalized frequency with diameter D and the reference velocity u_{ref} of 10 m/s.

In the left diagram the frequency (blue line) and the Kolmogorov -5/3 law (black line) in the location x/D=1 are displayed. The -5/3 law describes the usual behaviour of the isotropic area in a turbulent flow. A significant peak at St=1.9 is detected in the blue line. This is the frequency of 1p.
A similar curve is detected in the middle diagram, which describes the frequency in the position x/D=3. The right diagram shows the PSD in the location x/D=6 of the first modes without a significant peak.

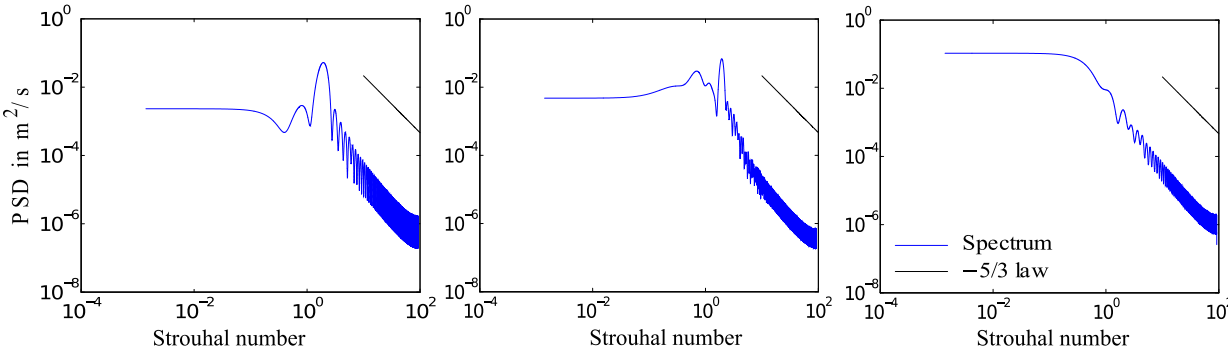

Figure 7. Spectra of the first time mode; Left: x/D=1; Middle: x/D=3; Right: x/D=6.

4. Discussion

By the means of a CFD analysis the full wake flow behind a turbine is calculated and the important characteristics of the wake flow are extracted to discuss the accuracy and the limits of the DDES with the sliding mesh method.

The general wake flow can be divided into two parts: the near wake, which includes the potential core and information about the tip vortex, and the far wake behind the potential core. At the beginning of this chapter the results of the streamwise velocity u(x,t), vertical velocity v(x,t) and the TKE in the y-z-plane of the near and far wake are discussed and compared with corresponding experimental measurements and results from literature.

A part of the near wake is displayed in figure 3, due to the clear circular structure and the low TKE level inside of the wake, which describes the potential core. In contrast to the measurement, the centre of the wake has a considerable lower TKE level. Furthermore, the TKE level in the ambient flow has the same value as in the centre of the deficit in both cases. This difference can be attributed to the inlet. Here the simulation starts with a TI about 1% instead of 12%. A reason for the too weak TI in the inflow is the used spectral synthesiser algorithm, which generated the TI in the inflow. On the other hand, a workgroup in the previous work by Bartl and Sætran [3] has successfully applied this method.

This mismatch can be a reason for the small difference of the velocity deficit. This assumption is based on an investigation by Bartl and Sætran [3]. They measured a significant asymmetrical velocity peak until u*=0.8 and a velocity deficit under 0.6 in the location x/D≈0.3, behind a turbine with the same rotor and a TI=0.24%.

In the next part of this study, the vertical velocity v* is compared to the measurement in the middle diagram of figures 3 and 4. One reason for the measurement in the near wake is negative vertical velocity in the inflow of the experiment. This influence may not be evident in the simulation and is a consequence of the method, which generates the shear flow in the experiment.

The next property of the near wake is the TKE. It corresponds with the measurement in the location of the maxima and is in the same range of the TKE level. A mismatch of the TKE level inside of the

wake can be explained by the low inflow TI. Also, Bartl and Sætran [3] measured a TKE under 0.01 in x/D≈3.

In the far wake the influence of the tip vortex dispersed and the shear flow increases inside of the wake. This process can be detected in the results of the position x/D=6. The streamwise velocities of the simulation and measurement describe a decreasing deficit, compared to the location x/D=3.

One difference is detected in the free stream velocity, which is higher than one, due to the blockage effect in the wind tunnel. The mesh grid next to the wind tunnel wall has a low mesh quality, due to the optimising of the computer performance, which could not calculate the increasing thickness of the boundary layer exactly. Similar to the first location, the vertical velocity overestimates the maximum and minimum peaks.

Finally, the TKE of the simulation corresponds well in level and location with the measurement. However, the TKE of the simulation indicates a higher spatial variation as the TKE of the measurement. Compared to the measurement the simulation has a short time average of one second.

The next part of this section discusses the coherent motion with the dissipation process of the fluctuation load. The velocity $\tilde{u}(x,t)$ demonstrates the vortex shedding of the tip vortices form the blade tips in the near wake. The Hot-Wire investigation by Lynum [6], located different tip vortices only in the distance x/D=1. They are in a range between r/D=0.55 and 0.62. The study by Eriksen und Krogstad [7] figured out the process of the coherent velocity in streamwise direction. They measured the tip vortices between r/D=0.55 and 0.59 in x/D=0.43 and a tip vortex r/D=0.42 and r/D=0.72 in x/D=3. The increasing structures, which are also detected in the POD of the DDES, are a consequence of the merged tip vortices in the distance x/D=3. Both studies used the same rotor and a low TI=0.24%. These locations of the tip vortex correspond with the results of the DDES. In addition, an indication of the root vortex is displayed in the left diagram of figure 6.

The dissipation process of the fluctuation load can be described with the significant frequency of 1p in the near wake compared to the far wake. Therefore, it is assumed that the coherent motion has the main frequency around 1p.

Eriksen [8] found out that the frequency of 1p has an influence on the flow until x/D=5. This study shows, that the frequency 1p is in the range about r/D=0 to 0.7525 in the location x/D=1 and in the location x/D=3 with a range about r/D=0.45 to r/D=0.9. The coherent motion of the simulation appears in these ranges.

The results demonstrate that the DDES is able to calculate the time-averaged velocity deficit, the flow rotation and mean turbulent kinetic energy in the wake, which show a good match with the experimental measurements of the same quantities. Furthermore, the simulation indicates the dissipation of the 1p-fluctuation, which correspond with previous studies. On the other hand, the full spectra and significant 3- frequencies are not detected in the first few modes. An explanation of this mismatch could be the dissipation of this frequency in front of the first operation point in x/D=1. Moreover, a numerical diffusion could possibly shift the energy contained in the 3p to 1p, which depends on the interaction between the resolution of the mesh behind the wind turbine and the bounded central difference scheme. On the other hand, no changes are detected with a higher grid resolution in this area.

5. Conclusion

This study revealed some significant aspects of wake modelling with DDES and the sliding mesh technique. The report examined the characteristics in the near and far wake area behind a turbine model.

The method was able to simulate the streamwise velocity, vertical velocity and the TKE behind a turbine at different downstream distances. The results of the simulation match well with the experimental results. Furthermore, the coherent motions and the significant frequency of the flow behind the turbine reflected the expected values compared to the literature. The coherent motion in the near wake exhibits a tip and root vortex and the dissipation process of significant frequency 1p.

However, the DDES differs from the experimental measurements in some points. In the near wake the nacelle has a significant impact on the velocity deficit and the vertical flow component is overestimated compared to the results of the experiment. Furthermore, the TKE has a lower level in the centre of the deficit and in the ambient air compared to the experiment.

In the far wake, the velocity and the TKE correspond with the experiment. In a few points the results of this work had a higher spatial variation than in the experiment, which might be due to the short simulation time. Furthermore, no dominant 3p-frequency is detected in the first few modes at the operating points. A number of possible reasons for the deviations in the DDES were discussed and should be investigated in more detail in a future study.

Consequently, it is proposed to improve the boundary conditions, a User-Define-Function should generate the TI in the inlet, the simulation should run for a longer time to produce a longer time average and the y_+ - value should be reduced under one to model the boundary layer exactly.

References

[1] Pionmelli, U., Balaras, E., Pasinato, H., Squires, K. D and Spalart, P.D. [2003], The inner-outer layer interface in large-eddy simulations with wall-layer models, *International Journal of Heat and Fluid Flow* **23**, 538-500

[2] Spalart, P.R, Jou, W. H, Strelets, M. and Allmaras, S. R. [1997], A new version of detached-eddy simulation, resistant to ambiguous grid densities. *Theoretical and Computational Fluid Dynamics, 20:181-195, 2006*

[3] Bartl, J. and Sætran, L. [2017], Blind test comparsion of the performance and wake flow between two in – line wind turbines exposed to different turbulent inflow conditions, *Wind energy science* **2**, 55-76

[4] Bartl, J., Mühle, F., Schottler, J., Sætran, L. Peinke, J., Adaramola, M. and Hölling M. [2017], Experiments on wind turbine wakes in yaw: Effects of inflow turbulence and shear. *Manuscript submitted to Wind Energy Science.*

[5] Chatterjee, A. [2000], An introduction to the proper orthogonal decomposition, *Computational Science* **78**, 808-817

[6] Lynum, S. [2013], Wind turbine wake meandering, *Master thesis at the NTNU*, url (2017): hdl.handle.net/11250/257551

[7] Eriksen, P. E. and Krogstad, P. [2017], Development of coherent motion in the wake of a model wind turbine, *Renewable Energy* **108**, 449-460

[8] Eriksen, P. E. [2016], Rotor wake turbulence: An experimental study of a wind turbine wake, *Doctoral thesis at NTNU 2017*: 2017:34, isbn: 978-82-326-1408-0